TOPICAL REVIEW — Fundamental physics research in lithium batteries

Li-ion batteries: Phase transition*

Peiyu Hou(侯配玉)[1], Geng Chu(褚赓)[2], Jian Gao(高健)[2], Yantao Zhang(张彦涛)[1], and Lianqi Zhang(张联齐)[1,†]

[1] *Tianjin Key Laboratory for Photoelectric Materials and Devices, School of Materials Science and Engineering, Tianjin University of Technology, Tianjin* 300384, *China*

[2] *Beijing National Laboratory for Condensed Matter Physics, Institute of Physics, Chinese Academy of Sciences, Beijing* 100190, *China*

(Received 5 June 2015; revised manuscript received 28 August 2015; published online 1 December 2015)

Progress in the research on phase transitions during Li^+ extraction/insertion processes in typical battery materials is summarized as examples to illustrate the significance of understanding phase transition phenomena in Li-ion batteries. Physical phenomena such as phase transitions (and resultant phase diagrams) are often observed in Li-ion battery research and already play an important role in promoting Li-ion battery technology. For example, the phase transitions during Li^+ insertion/extraction are highly relevant to the thermodynamics and kinetics of Li-ion batteries, and even physical characteristics such as specific energy, power density, volume variation, and safety-related properties.

Keywords: Li-ion batteries, phase transition, phase diagram, electrodes

PACS: 61.66.Fn, 61.50.Ah, 61.05.cp **DOI:** 10.1088/1674-1056/25/1/016104

1. Introduction

The phenomenon of phase transitions and the resultant phase diagrams in Li-ion batteries (LIBs) are often observed in the synthesis of materials, electrochemical reaction processes, temperature changes of batteries, and so on. Understanding those phenomena is crucial to design more desirable materials and facilitate the overall development of LIBs. For instance, if the conditions of phase transition such as sintering temperature or composition are well known, more excellent materials for LIBs can be designed and prepared.[1] Such knowledge is also beneficial for choosing an electrolyte that is more stable during the electrochemical reaction process.[2] Thermodynamics and kinetics of phase transition have to be discussed first, as far as the study of phase transition is concerned. It should also be noted that the investigations and understanding of those phase transitions in LIBs now from macro to micro and from thermodynamics to kinetics are gradually being realized on the basis of newly developed advanced characterization techniques. Thus, advanced study tools play a significant role in understanding phase transition clearly and in depth.

1.1. Thermodynamics of phase transition

The thermodynamics of phase transition may be used to estimate whether one kind of phase transition reaction can occur or not. Usually, transformations between different ordering structures or from ordered to disordered structure occur during the process of phase transition. Phase transitions were first classified by Paul Ehrenfest according to the continuity of thermodynamic potential as well as its derivative. Thermodynamic potential can be defined as $\Gamma = F + PV$, where F is free energy. The phase transitions during the electrochemical process in LIBs due to Li^+ extraction/intercalation have been investigated widely. For this kind of phase transition, Gibbs free energy is adopted. The most direct expression of thermodynamics can be described using the Nernst equation as follows:

$$\Delta_r G^s = -nFE^s.$$

Here, n is the quantity of transferred electrons per mole electrode materials in the oxidation or reduction reactions; F is the Faraday constant ($F = 96485$ C/mol); E^s is the thermodynamic equilibrium potential at the standard condition; and G is the Gibbs free energy of formation. Two kinds of phase transitions can usually be observed as electrochemical reaction types during the Li^+ extraction/intercalation process.

One is first-order phase transition, which typically appears in such electrode materials as $LiFePO_4$. Its charge–discharge curves can usually be presented as "L" shapes, indicating a clear potential plateau during Li^+ extraction/intercalation due to formation of a distinct new structural phase. The voltage can be calculated as follows:

$$\begin{aligned} LiFePO_4 &= x\mathrm{Li} + x\mathrm{FePO_4} + (1-x)\mathrm{LiFePO_4}, \\ \Delta_r G &= x\Delta_f G(\mathrm{Li}) + x\Delta_f G(\mathrm{FePO_4}) \\ &\quad + (1-x)\Delta_f G(\mathrm{LiFePO_4}) - \Delta_f G(\mathrm{LiFePO_4}) \\ &= x\Delta_f G(\mathrm{FePO_4}) - x\Delta_f G(\mathrm{LiFePO_4}) \\ &= -xFE, \\ E &= [\Delta_f G(\mathrm{FePO_4}) - \Delta_f G(\mathrm{LiFePO_4})]/(-F). \end{aligned}$$

*Project supported by the National High Technology Research and Development Program of China (Grant No. 2013AA050906) and the National Natural Science Foundation of China (Grant Nos. 51272175 and 21301127).

†Corresponding author. E-mail: tianjinzhanglq@163.com

© 2016 Chinese Physical Society and IOP Publishing Ltd

The second behaves as a second-order phase transition. A typical charge–discharge "S" shape curve is usually observed, meaning a continuous change in electrochemical potential due to continuous formation of solid solution phases. It can be seen in most of the range of Li^+ extraction/intercalation in $LiCoO_2$. The voltage can be calculated as follows:

$$\begin{aligned} LiCoO_2 &= xLi + Li_{1-x}CoO_2, \\ \Delta_r G &= \Delta_f G(Li_{1-x}CoO_2) - \Delta_f G(LiCoO_2) \\ &= -xFE, \\ E &= [\Delta_f G(Li_{1-x}CoO_2) - \Delta_f G(LiCoO_2)]/(-xF). \end{aligned}$$

1.2. Kinetics of phase transition

Phase transition can occur according to the thermodynamics, but this does not mean that the phase transition reaction can really be observed, due to the kinetics limitation. It is associated with the speed of the phase transition reaction. The speed of the electrochemical reaction during the process of Li^+ extraction/intercalation is not only related to intrinsic ionic and electronic transfer of materials, but is also related to the interface between electrode and electrolyte. It is a complex and continuous reaction process. The inferior kinetics during the process of Li^+ extraction/intercalation can cause huge polarization and thus an incomplete electrochemical reaction or even a disappearance of reaction. In order to improve the phase transition reaction speed of electrode materials, researchers have put forward many solutions, such as decreasing the size of the primary particle[3] and foreign element doping,[4] to improve the ionic and electronic conductivity of the electrode materials. However, the nanocrystallization method cannot solve all the polarization problems.[5] Until now, most of the research work on phase transition during the process of Li^+ extraction/intercalation has been performed from the aspect of thermodynamics. With the rapid development of modern advanced characterization tools, especially for micro-, nano- and *in situ* techniques, kinetic investigations of phase transition reactions are being realized gradually. Therefore, advanced characterization tools become more and more important for thoroughly understanding the nature of phase transition reactions.

2. Characterization methods of phase transition

Almost all the research methods used to study the material structure in other fields can also be applied to investigating the phase transitions of LIBs. Among them, x-ray diffraction (XRD) technology is the most direct method to distinguish the phase structure of LIBs materials. Thus, it has been widely used in researching phase analysis and studying phase transitions.[6] However, some special phase structures cannot be distinguished well by the diffraction method, so other local characterization methods such as Raman spectra have to be adopted.[7] Transmission electron microscopy (TEM) is also a powerful tool to get the microstructure information of materials, especially to obtain high spatial resolution.[8] Only recently could lithium ions be seen directly via electron microscope imagery, by using the spherical aberration correction electronic microscopy.[9] Some *in situ* experimental techniques are also being developed to understand in depth the structural changes of electrode materials during Li^+ extraction/insertion. The characterization methods now available for LIBs, with different spatial resolution levels, have been summarized,[10] as shown in Fig. 1. The nature of phase transition processes will be better described by combining those methods in the future.

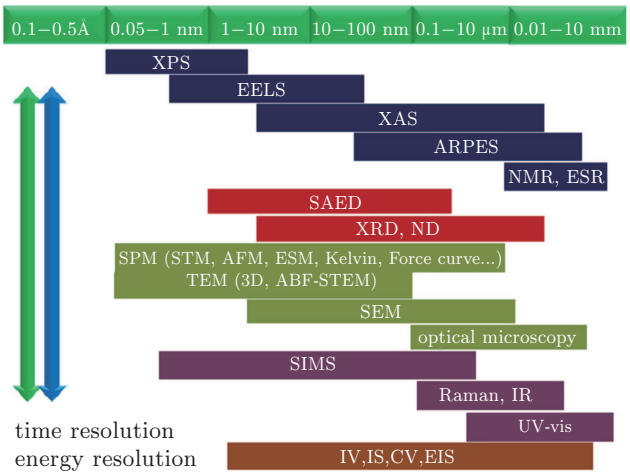


Fig. 1. Characterization techniques with different spatial resolution.[10]

Phase transitions can also be studied by such theoretical methods as first principles calculation. Theoretical calculations can guide us in developing new electrode materials,[11–13] optimizing structures of multiphase materials,[11] stabilizing the phase under different experimental conditions,[12,13] exploring the paths of reaction or decomposition,[14] etc. Some research results will be mentioned below. Ceder's group at M.I.T., by combining first principles calculations with a crystal structure database, calculated properties of a large number of LIB electrode materials. This kind of research is named the "materials genome initiative (MGI)".

Below, three typical electrode materials, $LiCoO_2$, $LiFePO_4$ cathode and Si anode, are taken as examples to illuminate the study of phase transitions during the process of Li^+ extraction/intercalation in LIBs from the viewpoints of thermodynamics, kinetics, and characterization methods.

3. Phase transition in typical cathode and anode materials

3.1. Layered $LiCoO_2$

The first commercialized cathode material of LIBs is the layered $LiCoO_2$, which still dominates the portable electric device market due to high volumetric density.[15,16] $LiCoO_2$ prepared by a conventional high-temperature solid state reaction method has an O3 structure in which the oxygen anion has a cubic close-packed arrangement in the form of ABCABC. During the electrochemical process, many complex phase transitions, especially in the lithium extraction stage are involved. In the past 30 years, plenty of investigations have focused on these phase transitions to understand the reactions and structural evolution mechanisms. The main investigations with respect to thermodynamics and dynamics are summarized here.

The pioneering work on identification of phase transitions during Li^+ insertion/extraction process was carried out by Dahn and Ohzuku *et al.*[17–19] As x varies from 1.0 to 0.3, Li_xCoO_2 evolves mainly in successive solid solution forms, which are considered to be second-order phase transitions. However, during the course, three first-order phase transitions are also clearly observed, as shown in Fig. 2. Two

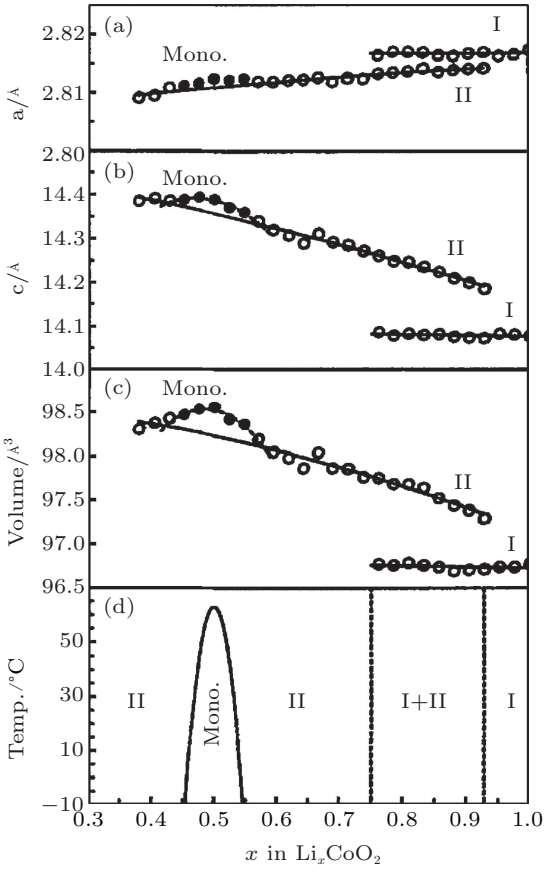


Fig. 2. Unit cell constants (a), (b) and cell volume (c) as functions of lithium concentration x in Li_xCoO_2, as well as a global phase diagram (d) based on the results (a)–(c) for Li_xCoO_2.[17]

first-order phase transitions occur at around $x = 0.5$, which are related to transformation between hexagonal II and monoclinic phases. The driving force for the phase transitions ($x = 0.5$) was found to come from the order/disorder transition of Li^+.[17,20] The third first-order phase transition happens in the range of $0.75 \leq x \leq 0.93$, which is ascribed to the electronic effect of transitional metal ions.[21,22] The experimental results show that the two phases were both of hexagonal crystal structure with similar lattice constants, based on the repeated XRD analysis of Li_xCoO_2 ($0.75 \leq x \leq 0.93$).[19] Delmas *et al.*[21] demonstrated that the two phases coexist for $0.75 \leq x \leq 0.93$, ascribed to a metal–insulator transition rather than structure. The metal–insulator transition was attributed to the electric effect of variation of Co^{3+} to Co^{4+}, from ^7Li MAS NMR results. Afterward, Ceder *et al.*[22] identified the mechanism of this previously anomalous metal–insulator transition as a Mott transition of impurities, via density functional theory (DFT) calculations on large supercells. DFT calculations reveal that for dilute Li-vacancy concentrations the vacancy binds a hole and forms impurity states, yielding a Mott insulator.

The phenomenon of phase transitions occurring in Li_xCoO_2 in the low Li content range ($0 \leq x \leq 0.5$) are somewhat difficult to make clear according to the reports.[17–28] The earlier works by Ohzuku and Ueda[19] indicate that the reaction proceeds in a topotactic manner, i.e., two-phase reactions ($0 < x < 1/4$ and $3/4 < x < 1$) and a single-phase reaction ($1/4 < x < 3/4$) in Li_xCoO_2. Another monoclinic phase ($a = 4.91$ Å, $b = 2.82$ Å, $c = 5.02$ Å, and ß = 111.4°) was observed in $1/4 < x < 0$ in addition to that at about $x = 0.55$ ($a = 4.90$ Å, $b = 2.81$ Å, $c = 5.05$ Å, ß = 108.3°). Possible lithium ordering at $x = 1/4$ and 3/4 for this type of material was described in terms of a [2×2] superlattice in a triangular lattice of sites. In 1996, structural characterization of Li_xCoO_2 with x values was studied for the first time via *in situ* x-ray diffraction.[23] The analysis reveals that as x approaches 0 an increase in crystallographic quality occurs, rather than the expected destruction of the core structure of Li_xCoO_2 by a drastic increase in structural disorder. For the first time, the end member CoO_2 phase was isolated and detected. This CoO_2 phase was certified to be a hexagonal single-layered phase (O1 stacking, Fig. 3(a)) and had lattice parameters of $a = 2.822$ Å and $c = 4.29$ Å. These results are well supported by theoretical calculations from Ceder's group.[24] Ceder *et al.* investigated phase transitions in the layered oxide Li_xCoO_2 in a larger range ($x \leq 0.4$) by first principles calculation, giving such different structural types as O1, O3, and H1-3 according to oxygen stacking manner and Li occupation sites, as seen in Figs. 3(a)–3(c). As to common $LiCoO_2$, the oxygen planes are stacked according to an ABCABC arrangement, and the host is conventionally referred to as O3 (Fig. 3(b)). Amatucci

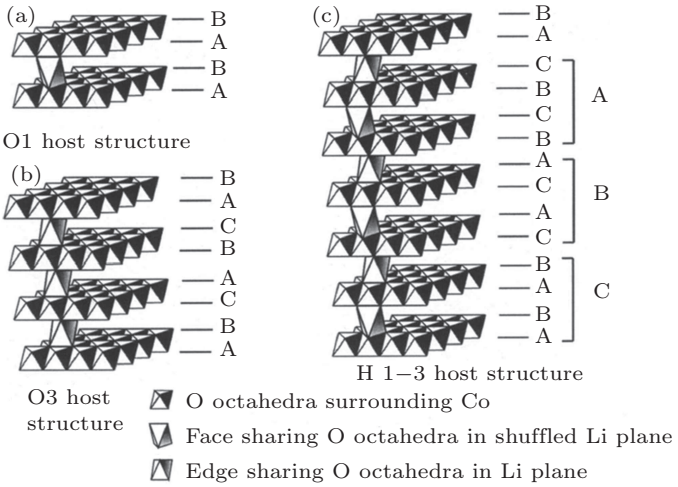


Fig. 3. Schematic illustration of the three host structures of Li_xCoO_2: O1 (a), O3 (b), and H1-3 (c). The vertices of the octahedra correspond to oxygen ions. Upper case letters describe the stacking of the close-packed oxygen layers. (d) Free energy curves as a function of Li concentration at $T = 30°$; regions separated by vertical dashed lines indicate the concentration intervals in which different host structures are stable.[24]

et al.[23] have verified that O3 is unstable, as it is completely deintercalated, and the hexagonal form of CoO_2(referred to as O1) with an ABAB oxygen stacking is obtained, which is consistent with calculated results.[24] A hybrid of O3 and O1, named H1-3 (Fig. 3(c)), is also deduced to be a stable phase. A predicted phase diagram of Li_xCoO_2 on the basis of a series of phase transitions during Li^+ extraction/insertion process is suggested, as displayed in Fig. 3(d). For Li concentrations between $x = 0$ and 0.12, the O1 form of CoO_2 coexists with H1-3 having a Li concentration of $x = 0.12$. While Li concentrations vary between 0.12 and 0.19, H1-3 is stable as a single phase. In the concentration range from 0.19 to 0.33, H1-3 coexists with O3 phase. When x is over 0.33, only O3 phase appears. However, with a continuous increase of x, other new phases based on the O3 structure can be observed, due to Li^+ order/disorder or electronic effects.[17–22]

In addition to thermodynamically stable O3 host structures for $LiCoO_2$, a thermodynamically metastable O2-structured $LiCoO_2$ was also demonstrated to exist by experimental and theoretical studies.[25–27] Unlike the O3 structure, the O2 structure must be prepared by the ion-exchange route. In the O2 structure, such new phases as T#2, T#2' and O6 have been proposed. Usually, a phase transition between O3 and O2 structures is believed to be impossible. Nevertheless, Lu *et al.*[28] first observed O2-Li_xCoO_2 in the phase diagram of O3-$LiCoO_2$ using spherical aberration-corrected scanning transmission electron microscopy (STEM) with high-angle annular-dark-field (HAADF) and annular-bright-field (ABF) techniques. Furthermore, in Lu's work, O1, O2, and O3 structures were all detected clearly on the basis of HAADF micrographs, as indicated in Fig. 4. Some different information on phase transitions for Li_xCoO_2 in the range of $0.5 \leq x \leq 1$ were presented. The detailed phase transformation of Li_xCoO_2 ($0.5 \leq x \leq 1$) is revealed in Fig. 4(e). Recently, direct

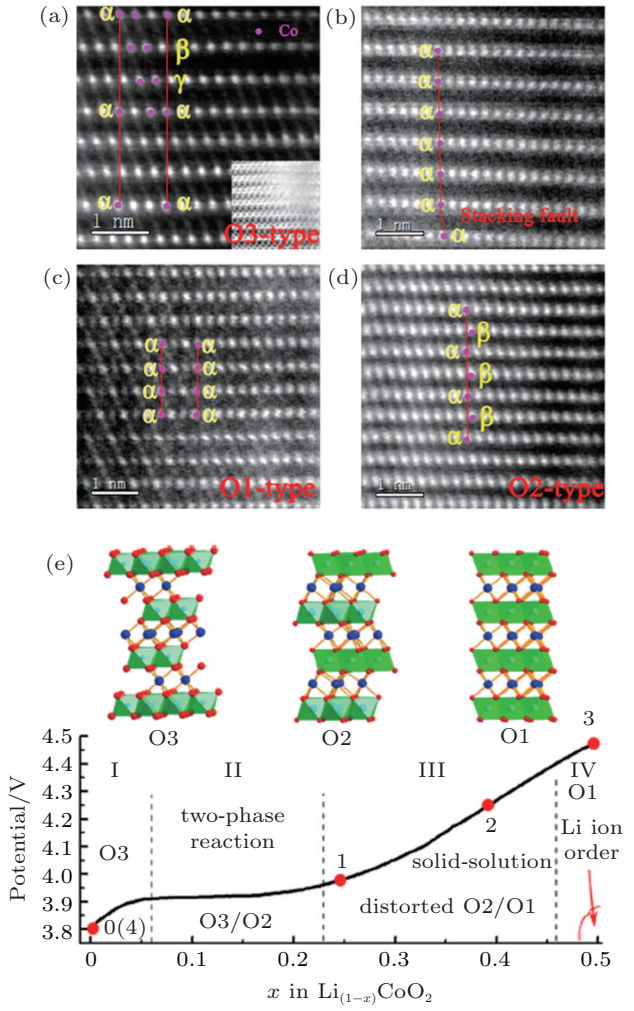


Fig. 4. STEM-HAADF images of surface structure: (a) pristine $LiCoO_2$, (b) $LiCoO_2$ charged to 4.2 V, (c) charged to 4.5 V, and (d) discharged to 3.0 V at the [010] zone axis. (e) Phase diagram of Li_xCoO_2 ($1 \leq x \leq 0.50$) nanoparticle. Numerical symbols 0-4 represent the sample points for STEM observation: (0) pristine $LiCoO_2$, (1) charged to 3.9 V, (2) charged to 4.2 V, (3) charged to 4.5 V, and (4) back to 3.0 V.[28]

observation of delithiated structures of Li_xCoO_2 at atomic scale has become available due to the rapid development of

STEM with HAADF and ABF techniques. The phase and structure evolution in a highly delithiated state Li_xCoO_2 ($x \leq 0.5$) is more important than that of $x \geq 0.5$ for achieving higher capacity and energy density to meet the increasing demands for LIBs. Advanced STEM with HAADF and ABF techniques is a new method for researching lithium storage and structure evolution mechanisms in this important LIB cathode material.

We have mainly discussed the phase transitions from the thermodynamics view. However, whether the phase transition can be observed clearly or even occur at all sometimes depends strongly on kinetic factors such as electric conductivity and Li^+ chemical diffusion coefficient versus Li^+ concentration in Li_xCoO_2. Some research activities in those aspects have been performed. Brake *et al.*[29] studied the variation of the Li^+ diffusion coefficients for Li_xCoO_2 as a function of the lithium concentration during the lithium insertion reaction. Kinetics investigation reveals that the average diffusion coefficient for the composite Li_xCoO_2 is in the range of 10^{-9} $cm^2 \cdot S^{-1}$, indicating relatively uncomplicated reaction kinetics for the lithium insertion reaction. The variation of the diffusion coefficient in the insertion range $0.3 < x < 0.85$ is consistent with filling/removal of Li^+ from a single site within the host lattice over this particular composition range. At a composition of around $x = 0.65$, the diffusion coefficient reaches a local minimum. Within the compositional range described, there exists a two-phase system with the phase transition.[17]The structural rearrangement therefore takes place as lithium is inserted or extracted from lattice sites. Subsequently, Ven *et al.*[30] investigated the mechanisms of Li^+ diffusion in Li_xCoO_2 via first principles and found that Li^+ diffusion occurs predominantly by a divacancy mechanism. The calculation of the diffusion coefficient at 400 K with kinetic Monte Carlo simulations shows that diffusion efficiency initially increased by several orders of magnitude with x as a result of the decrease in activation barrier with x, as indicated in Fig. 5. Li^+ ordering at $x = 0.5$ produces a dip in the diffusion coefficient. As x increases beyond 0.65, the diffusion coefficient drops, owing to the decreasing concentration of divacancies.

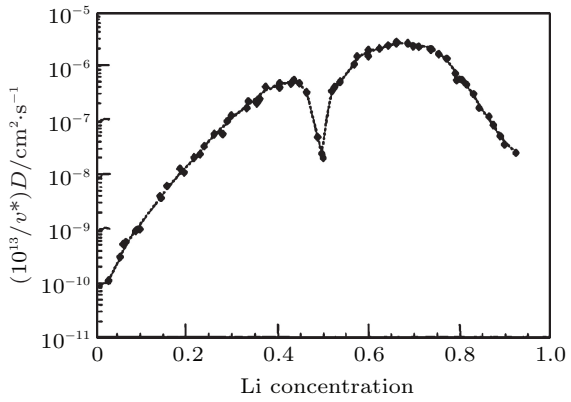


Fig. 5. Calculated diffusion coefficient (D) with lithium concentration, x in Li_xCoO_2.[30]

3.2. Olivine $LiFePO_4$

Olivine-type $LiFePO_4$, proposed by Goodenough *et al.*[31,32] in 1997, has achieved considerable attention due to the chemical stability, safety characteristics, environment-friendliness and low cost. The crystal structure of $LiFePO_4$ can be viewed as an ABAB oxygen sublattice with Li, Fe, and P occupying a subset of octahedral and tetrahedral interstitial sites respectively, having the space group of Pmnb with the following unit-cell parameters: $a = 6.011(1)$ Å, $b = 10.338(1)$ Å, $c = 4.695(1)$ Å.[33–36] Improving the rate capability of $LiFePO_4$ is scientifically interesting and practically significant because of its electronic insulator and mediocre ionic transport property.[37–42] Next, recent achievements with regard to phase separation and structural evolution mechanisms of $LiFePO_4$ involving thermodynamics and kinetics during the Li^+extraction/intercalation process are summarized.

To our knowledge, in terms of the electrode materials, the large variations of Li^+ concentration always lead to phase transformations during the charge and discharge processes, such as order–disorder transitions, crystallographic changes and two-phase reactions.[43] When cycling at room temperature for $LiFePO_4$, the Li^+ extraction from a lithiated triphylite phase, $LiFePO_4$, occurs through a first-order phase transformation to a delithiated heterosite phase, $FePO_4$.[44] Phase transformation research has focused on the $LiFePO_4/FePO_4$ two-phase transition and the existence of $Li_\alpha FePO_4$ and $Li_{1-\beta}PO_4$ solid solutions.[45] In order to understand the two-phase reaction in $LiFePO_4$, Andersson *et al.*[46] introduced two models: "radial model" and "mosaic model". Both models pinpoint the inactive $LiFePO_4$ unconverted in the charge process as the essence of lost capacity in the system. Srinivasan *et al.*[47] developed a "shrinking core" mathematical model to study the cause of low power capacity as shown in Fig. 6(a). During the charge and discharge processes, the single-phase core (e.g., fully charged $FePO_4$) was covered with the second-phase shell (e.g., discharge $LiFePO_4$) with transportation of Li^+, accompanying the phase boundary movement. The 'domino-cascade model' in Fig. 6(b) was experimentally observed by Delmas *et al.* through layer-by-layer intercalation in $LiFePO_4$ and used to illuminate the reasons for the high rate performance of the batteries with the poor electronic and ionic conductors, $FePO_4$ and $LiFePO_4$.[48] These models are introduced on the basis of steady state. The interpretations of the phase transformations vary according to particle shape and size, the (de)lithiation method, and the characterization method.[49]

In contrast to the well-documented two-phase nature of Li_xFePO_4 at room temperature, Delacourt *et al.*[50] and Dodd *et al.*[51] summarized the phase diagrams shown in Fig. 7 via temperature-controlled XRD, respectively. A solid solution Li_xFePO_4 ($0 \leq x \leq 1$) at an elevated temperature transforms

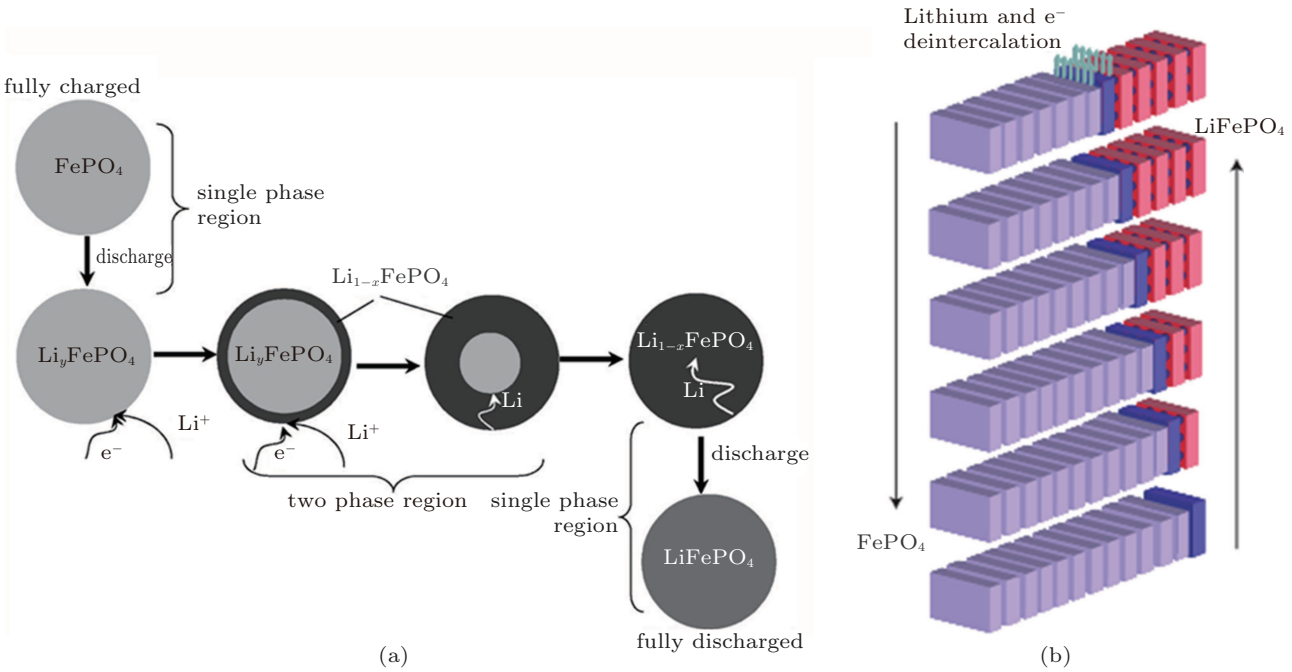


Fig. 6. Illustration of (a) shrinking-core model with the two phases and the movement of the phase boundary.[47] (b) Layered view of the 'domino-cascade' mechanism of the lithium deintercalation/intercalation mechanism in a $LiFePO_4$ crystallite.[48]

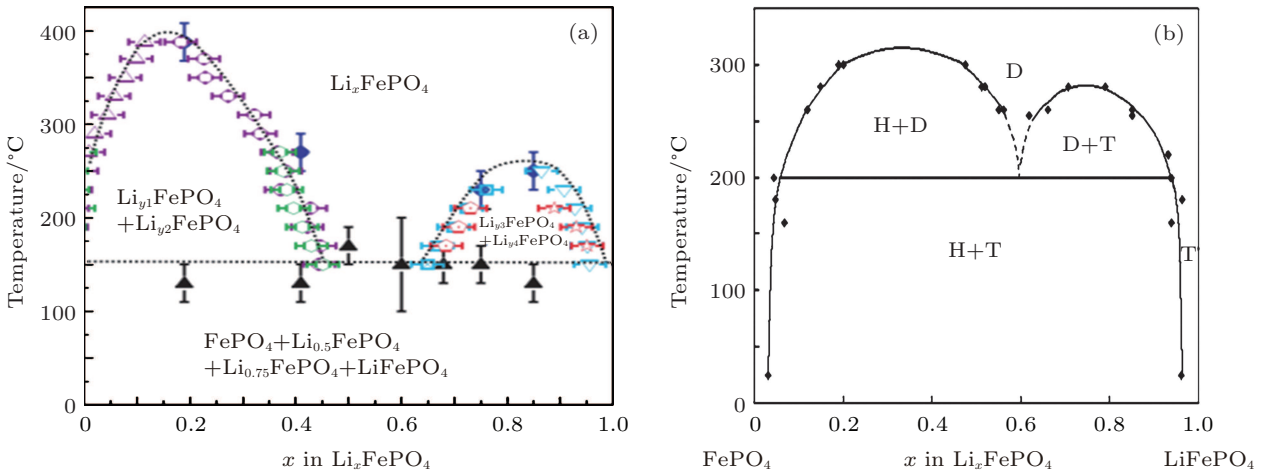


Fig. 7. (a) Phase distribution diagrams of Li_xFePO_4 ($0 \le x \le 1$) established from temperature-controlled XRD data.[50] (b) Phase diagram of $LiFePO_4$ (T, for triphylite), $FePO_4$ (H, for heterosite), and the merging new solid solution (D, for disordered).[51]

into a two-phase mixture between $LiFePO_4$ and $FePO_4$ as the temperature cools down. Beyond the contributions of temperature, particle size, geometry and composition,[49] the coherency strains can also be responsible for stabilizing intermediate solid solutions of Li_xFePO_4.[52]

Chen *et al.*[53] developed a phase evolution mechanism in which $LiFePO_4$ is transformed into isostructural $FePO_4$, using electron microscopic methods on chemically delithiated $LiFePO_4$. The results show that the lithium is extracted at narrow, disordered transition zones on the *ac* crystal surface and a substantial lattice mismatch caused cracks to form in the *bc* plane, leading to a newly created $FePO_4$ phase, as shown in Fig. 8(a). A microscopic mechanism of the phase transition from $LiFePO_4$ to $FePO_4$ was proposed by Gu *et al.*[54] Lithium cations in $LiFePO_4$ were directly detected at atomic resolution by an aberration-corrected annular-bright-field (ABF) scanning transmission electron microscopy (STEM). The pristine, fully charged and half charged states refer to $LiFePO_4$, $FePO_4$ and $Li_{0.5}FePO_4$, respectively, as seen in Fig. 8(b1)–8(b3). Subsequently, Orikasa[55] provided the first experimental observation of a Li_xFePO_4 metastable phase using time-resolved XRD, as shown in Fig. 9(a). This indicates that the new Li_xFePO_4 ($x = 0.6$–0.75) transient phase with the estimated lifetime of about 30 min rapidly transforms to the stable $LiFePO_4$ and $FePO_4$. The high rate performance of $LiFePO_4$ can be attributed to the metastable phase transformation path displayed in Fig. 9(b), which suggests a fast phase transition. Compared with the model based on relaxed states (white

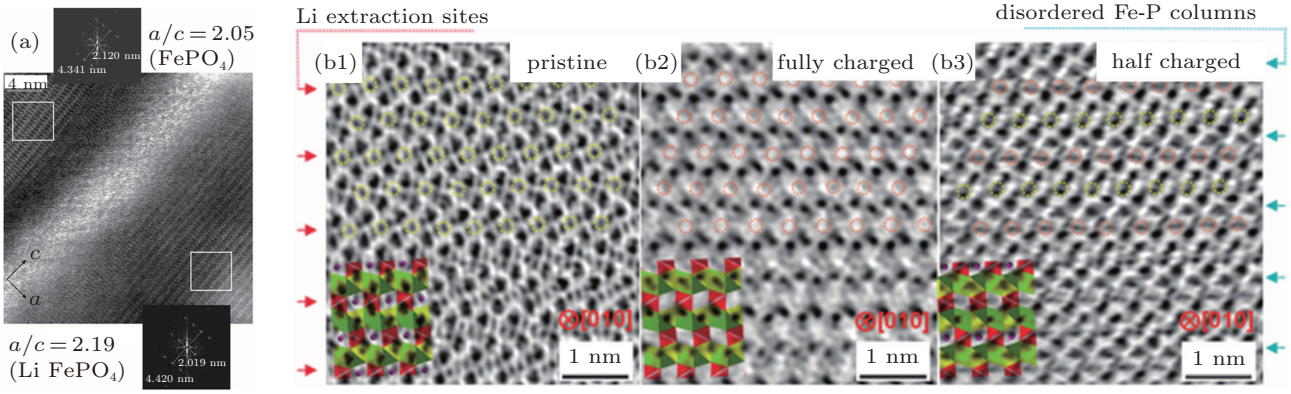


Fig. 8. (a) HRTEM image of the disordered region between two phases in $Li_{0.5}FePO_4$ crystal with Fourier transforms of the indicated areas.[53] ABF micrographs of (b1) pristine ($LiFePO_4$), (b2) fully charged ($FePO_4$) and (b3) half charged ($Li_{1-x}FePO_4$, $x = 0.5$) materials with the corresponding atomic structure shown in inset. Li sites are marked by yellow circles, and the delithiated sites are marked by orange circles.[54]

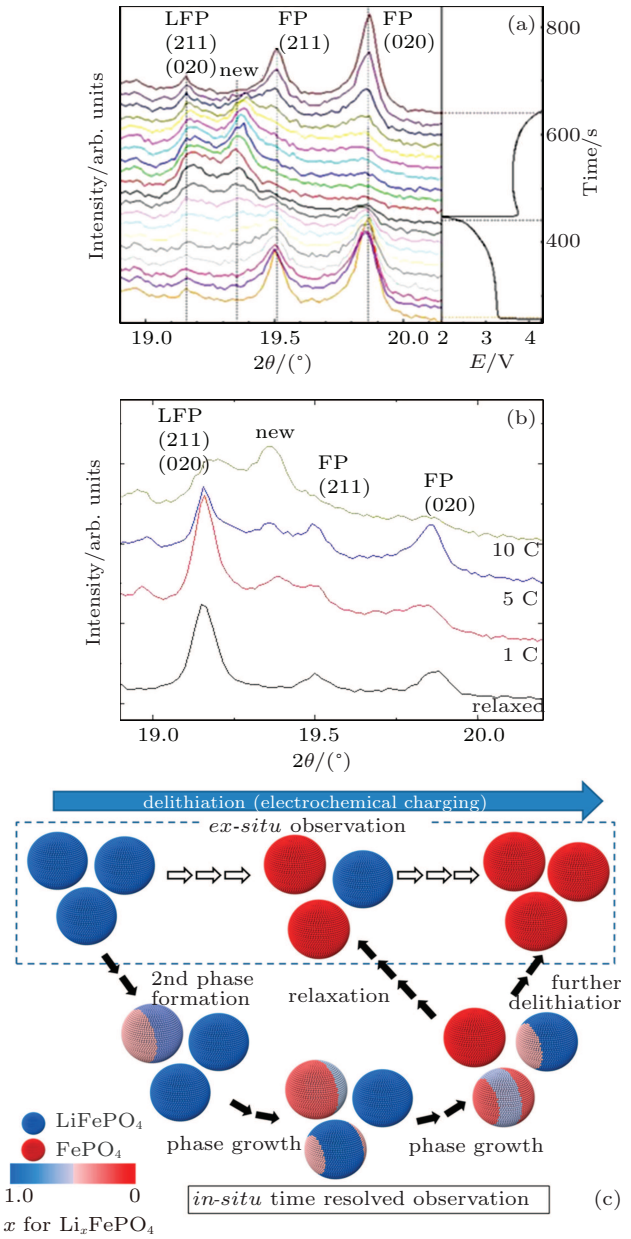


Fig. 9. (a) Detailed XRD patterns and the first discharge and second charge curves (right). (b) Time-resolved XRD patterns at the end of the first discharge state at different current densities. "Relaxed" represents the pattern of the sample relaxed for 1 day after 10 C charge and discharge cycles.[55] (c) Phase transition model of Li_xFePO_4.[56]

arrow path in Fig. 9(c)), the mechanism of Li_xFePO_4 is gradually transformed into the thermodynamically stable $FePO_4$ phase as further charged (black arrow path in Fig. 9(c)).[56]

We have reviewed some phase transition mechanisms in $LiFePO_4$. However, the occurrence of the phase-transition mechanisms also strongly depends on the limitation of the diffusion of Li^+ between the two-phase interfaces. This is related to electrochemical kinetics. Thus, the crystal structure of the compound often plays an essential role in determining the shape of the voltage profile as a function of Li concentration, which is related to the kinetic behavior of the material. First-principles statistical mechanical approaches can be applied to study the chemistry and crystal structures that give rise to kinetic properties.[57] A flat voltage plateau ($LiFePO_4$, at 3.45 V versus Li/Li^+) caused by two-phase electrochemical reaction can be verified from the Gibbs free energy according to the suggestions of Van der Ven *et al.*[58]

Sun *et al.*[59] employed DFT calculations to demonstrate that the stage-II configuration in delithiated $LiFePO_4$ is a thermodynamically metastable but kinetically controlled state. A dual-interface model was introduced to describe the delithiation mechanism of $LiFePO_4$ upon charging (Fig. 10).

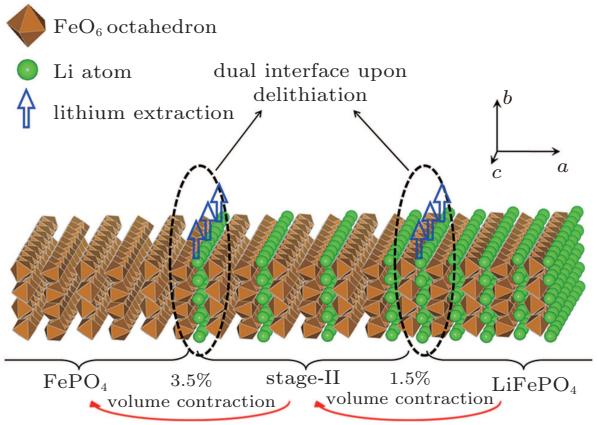


Fig. 10. Schematic view of possible models for the electrochemical delithiation process of $LiFePO_4$.[59]

Yu *et al.*[60] investigated the rapid delithiation behavior of $LiFePO_4$ by quick x-ray absorption spectroscopy and dynamically monitored the two-phase transition behavior. As depicted in Fig. 11(c), 90% of $LiFePO_4$ has been converted to $FePO_4$ after 120 seconds of chemical delithiation. Electrochemical delithiation of $LiFePO_4$ should be similar to chemical delithiation if the electron transport in both $LiFePO_4$ and $FePO_4$ is faster than ion transport. Compared with Fig. 11(e), linear combination fitting (LCF) results indicate that more than 60% of Li^+ can be extracted in either the chemical or electrochemical delithiation reactions. This similar kinetic property verifies that the Li^+ transport is the main governing factor for both reactions. Besides, the Johnson–Mehl–Avrami–Kolmogorov (JMAK) equation $f = 1 - \exp(-kt)^n$ (f: the fraction of $FePO_4$, k is a rate constant, and n relies on the phase growth geometry) can be used to analyze the kinetics of the phase transition from $LiFePO_4$ to $FePO_4$.

The two-phase transformation from $LiFePO_4$ to $FePO_4$ can be studied in samples with different morphology, particle size and surface coatings, and compared in either chemical or electrochemical delithiation reaction time, and so on.[61]

3.3. Silicon anode

Due to their high specific capacity, some anode materials such as Si, Ge, and Sn (as well as alloys containing these elements) attract much attention. Silicon is considered to be the next-generation anode material because of having the highest theoretical capacity (4200 mAh/g) as well as being environmentally benign, naturally abundant, and so on.

A series of alloys of Si and Li were developed,[62–66] which often resulted in a typical Li–Si diagram as shown in Fig. 12. In 2000, Li *et al.*[67] investigated the mechanism of Li^+ storage in silicon at room temperature, using silicon particles and nanowires. They found that crystalline silicon gradually changes to an amorphous silicon–lithium alloy with insertion of Li^+, and subsequent extraction of Li^+ can promote

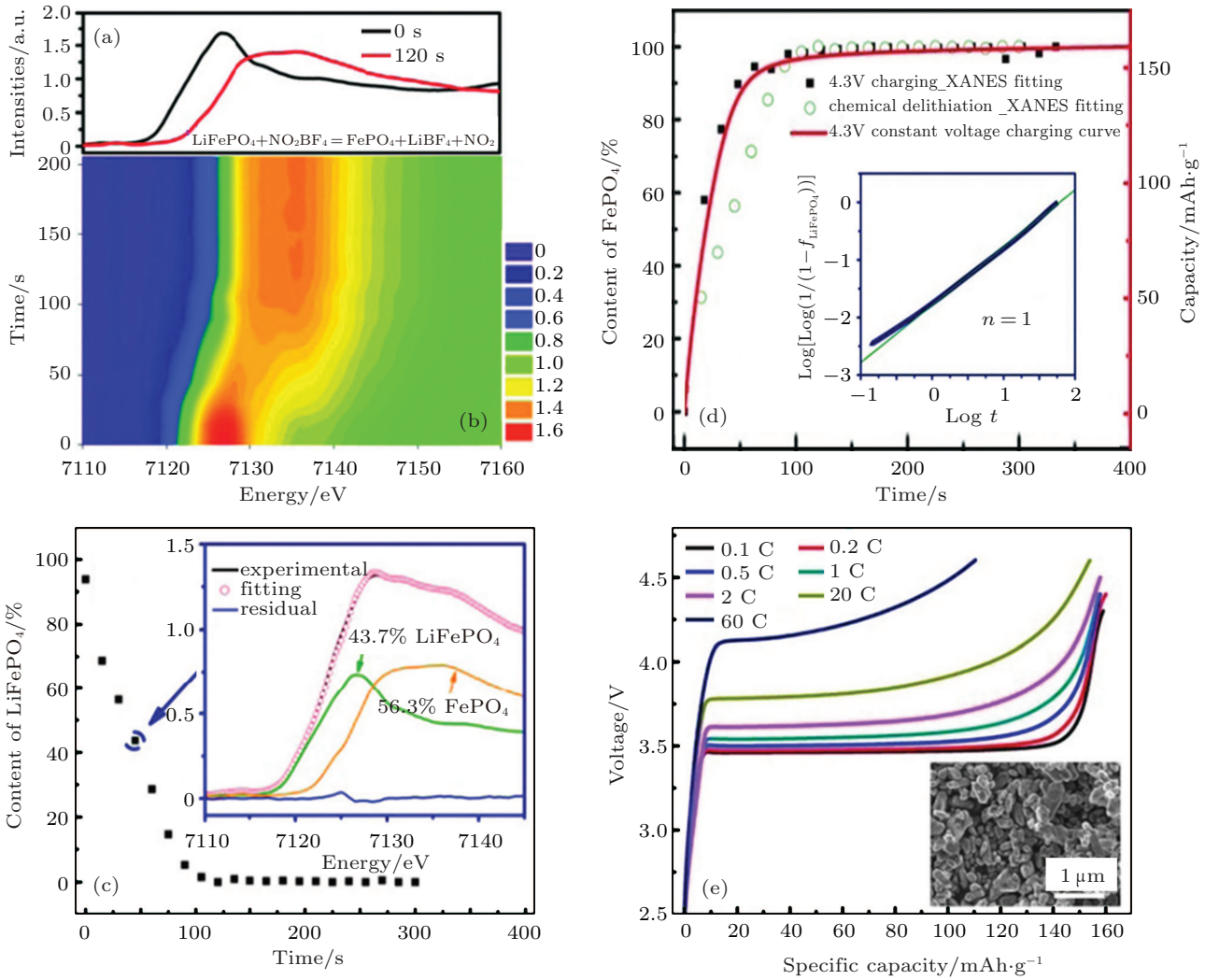


Fig. 11. (a) Fe K-edge XANES spectra of pristine $LiFePO_4$ and after 120 seconds of chemical delithiation; (b) the evolution and (c) linear combination fitting of Fe K-edge XANES spectra. (d) Comparison of fast delithiation of $LiFePO_4$ between *in situ* chemical delithiation and 4.3 V constant voltage charging; solid square symbols represent the $FePO_4$ content, the red solid line is the charge capacity of 4.3 V constant voltage charging. Inset: determination of the Avrami exponent with the Johnson–Mehl–Avrami–Kolmogorov equation; (e) charge curve of $LiFePO_4$ at different C rates.[60]

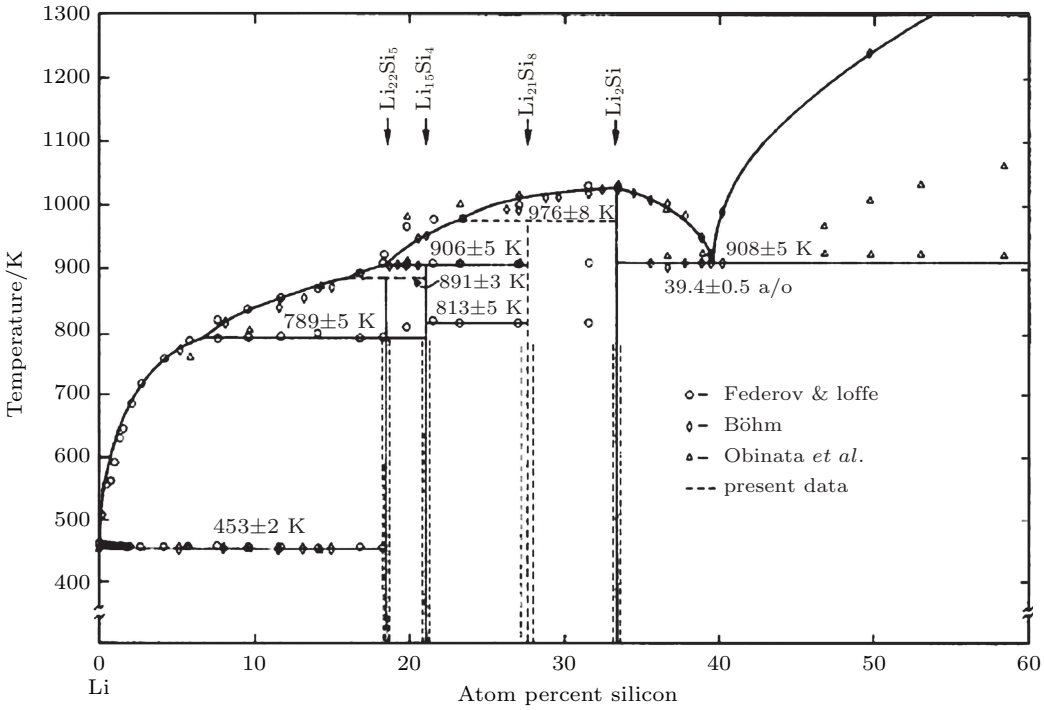


Fig. 12. Phase diagram of lithium–silicon system.[63]

recrystallization of amorphous Si. In 2003, Chiang *et al.* further reported an electrochemical mechanism driving crystalline silicon to amorphous phase during the insertion of Li^+.[68] In 2004, Obrovac *et al.* used *ex situ* XRD to demonstrate an amorphous phase arising from crystalline Si on one hand; on the other hand, they also observed the further formation of $Li_{15}Si_4$ crystalline phase as the discharge voltage lowers to 50 mV.[69] In the same year, Dahn *et al.* adopted *in situ* XRD methods to study structural change of amorphous silicon films in the charge and discharge process and also found the formation of $Li_{15}Si_4$ crystalline phase.[70] This result was also verified by Grey using nuclear magnetic resonance (NMR).[71,72] Additionally, Mao *et al.* used *in situ* transmission electron microscopy to find the movement of the phase boundary between amorphous silicon (a-Si) and amorphous Li_xSi ($x \sim 2.5$).[8] In summary, the specific reaction mechanism of crystalline Si can be described as follows:[73] during the initial discharge process:

$$\text{Si (crystalline)} + x\text{Li}^+ + x\text{e}^- \rightarrow \text{Li}_x\text{Si (amorphous)} + (3.75-x)\text{Li}^+ + (3.75-x)\text{e}^- \quad (1)$$

$$\rightarrow \text{Li}_{15}\text{Si}_4\text{(crystalline)}, \quad (2)$$

during initial charge process:

$$\text{Li}_{15}\text{Si}_4 \text{ (crystalline)} \rightarrow \text{Si (amorphous)} + y\text{Li}^+ + y\text{e}^- + \text{Li}_{15}\text{Si}_4 \text{ (residual)}. \quad (3)$$

Carbon coating has been investigated to improve the electrochemical performance of silicon anodes. Generally, it is believed that a carbon coating layer can restrain the merging or agglomeration of silicon nanoparticles and accelerate the lithiation rate, due to improving electron and ion transport.[74–76] Additionally, it is well known that upon lithiation, both crystalline and amorphous silicon transform to an amorphous Li_xSi phase, which subsequently crystallizes to (Li, Si) crystalline compounds, either $Li_{15}Si_4$ or $Li_{22}Si_5$.[76] The latter phase transition from amorphous Li_xSi to crystalline phase results in the huge volume expansion, which is responsible for the electrochemical degradation of silicon anodes. As to the carbon-coated silicon, the carbon layer is likely to partly restrain the formation of a crystalline compound, either $Li_{15}Si_4$ or $Li_{22}Si_5$, in that the toughness of carbon can prevent extreme volume change in a Si anode. In other words, the carbon coating layer helps suppress the phase transition from amorphous Li_xSi to a crystalline compound.

Most references report such strategies as carbon-coating or forming composite materials to be effective in improving the electrochemical performance of Si anodes. In our opinion, a double structured silicon anode, core-shell or yolk-shell structured, in which the interior section is porous coated silicon nanoparticles or a Si/C composite and the shell is a superior layer of Li^+ and an electron conductor with a stable structure, may be proposed to better enhance the electrochemical properties of silicon anodes.

Another interesting phase transition occurs during the electrochemical lithium extraction/insertion of the anode material β-SnSb alloy.[77,78] Li *et al.* synthesized nanosized β-SnSb and found that the lithium first reacted with Sb atoms to form Li_2Sb and Li_3Sb, and then the remaining Sn atoms were aggregated. After all the Sb changed into Li_3Sb, the Li–Sn alloy appeared. In the delithiation process, the reverse steps occur. This special mechanism was clarified by *ex situ* XRD.

4. Summary and outlook

Phase transition reactions are often observed in LIBs. No matter whether they occur in the synthesis of materials or in the process of electrochemical Li^+ extraction/intercalation, comprehensive and in depth understanding of the phenomena will significantly promote the technology of LIBs. Currently, most research in this field is carried out from macro-scale and thermodynamic viewpoints. In the near future, investigations from micro- or nano-scale and dynamics viewpoints should be empowered by the rapid development of modern advanced characterization methods. At present, high-throughput calculation is utilized to explore potential LIB materials, which will accelerate the research course of new phase materials. High spatial resolution, temporal resolution and energy-resolution technologies are also widely used to study the structure, composition and evolution of the bulk phase, surface phase and interface phase of materials. Some *in situ* tools are also being made better and better.

References

[1] Luo C H and Martin M 2007 *J. Mater. Sci.* **42** 1955
[2] Tatsumisago M, Hama S, Hayashi A, Morimoto H and Minami T 2002 *Solid State Ion.* **154** 635
[3] Yamada A, Chung S C and Hinokuma K 2001 *J. Electrochem. Soc.* **148** A224
[4] Chung S Y, Bloking J T and Chiang Y M 2002 *Nat. Mater.* **1** 123
[5] Zhong K F, Zhang B, Luo S H, Wen W, Li H, Huang X and Chen L 20011 *J. Power Sources* **196** 6802
[6] Feng G X, Li L F, Liu J Y, Liu N, Li H, Yang X Q, Huang X J, Chen L Q, Nam K W and Yoon W S 2009 *J. Mater. Chem.* **19** 2993
[7] Amdouni N, Zaghib K, Gendron F, Mauger A and Julien C M 2006 *Ionics* **12** 117
[8] Wang J W, He Y, Fan F, Liu X H, Xia S, Liu Y, Thomas H C, Li H, Huang J Y, Mao S X and Zhu T 2013 *Nano Lett.* **13** 709
[9] Gu L, Zhu C B, Li H, Yu Y, Li C, Tsukimoto S, Maier J and Ikuhara Y 2011 *J. Am. Chem. Soc.* **133** 4661
[10] Gao J, Lv Y and Li H 2013 *Energy Storage Science and Technology* **2** 250
[11] Kang B and Ceder G 2009 *Nature* **458** 190
[12] Ong S P, Chevrier V L, Hautier G, Jain A, Moore C, Kim S, Ma X and Ceder G 2011 *Energy Environ. Sci.* **4** 3680
[13] Chen H L, Hautier G, Jain A, Moore C, Kang B, Doe R, Wu L, Zhu Y, Tang Y and Ceder G 2012 *Chem. Mater.* **24** 2009
[14] Ong S P, Wang L, Kang B and Ceder G 2008 *Chem. Mater.* **20** 1798
[15] Mizushima K, Jones P C, Wiseman P J and Goodenough J B 1980 *Mat. Res. Bull.* **15** 783
[16] Kang K, Meng Y S, Breger J, Grey C P and Ceder G 2006 *Science* **311** 977
[17] Reimers J N and Dahn J R 1992 *J. Electrochem. Soc.* **139** 2091
[18] Reimers J N, Dahn J R and Vonsacken U 1993 *J. Electrochem. Soc.* **140** 2752
[19] Ohzuku T and Ueda 1994 *J. Electrochem. Soc.* **141** 2972
[20] Shao H Y, Levasseur S, Weill F and Delmas C 2003 *J. Electrochem. Soc.* **150** A366
[21] Menetrier M, Saadoune I, Levasseur S and Delmas C 1999 *J. Mater. Chem.* **9** 1135
[22] Marianetti C A, Kotliar G and Ceder G 2004 *Nat. Mater.* **3** 627
[23] Amatucci G G, Tarascon J M and Klein L C 1996 *J. Electrochem. Soc.* **143** 1114
[24] Van D V A, Aydinol M K and Ceder G 1998 *J. Electrochem. Soc.* **145** 2149
[25] Carlier D, Van der Ven A, Delmas C and Ceder G 2003 *Chem. Mater.* **15** 2651
[26] Delmas C, Braconnier J J and Hagenmuller P 1982 *Mater. Res. Bull.* **17** 117
[27] Carlier D, Saadoune I, Croguennec, Menetrier L M, Suard E and Delmas C 2001 *Solid State Ionics* **144** 263
[28] Lu X, Sun Y, Jian Z, He X, Gu L, Hu, Y S, Li H, Wang Z, Chen W, Duan X, Chen L, Maier J, Tsukimoto S and Ikuhara Y 2012 *Nano Lett.* **12** 6192
[29] Barker J, Pynenburg R, Koksbanc R and Ssidi M Y 1996 *Electrochim. Acra* **41** 248
[30] Van der Ven A and Ceder G 2001 *J. Power Sources* **97** 529
[31] Padhi A K, Nanjundaswamy K S and Goodenough J B 1997 *J. Electrochem. Soc.* **144** 1188
[32] Padhi A K, Nanjundaswarmy K S, Masquelier C, Okada S and Goodenough J B 1997 *J. Electrochem. Soc.* **144** 1609
[33] Van der Ven A, Bhattacharya J and Belak A A 2013 *Acc. Chem. Res.* **46** 1216
[34] Santoro R P and Newman R E 1967 *Acta Crystallogr.* **22** 344
[35] Andersson A S and Thomas J O 2001 *J. Power Sources* **97** 498
[36] Rousse G, Rodriguez-Carvajal J, Patoux S and Masquelier C 2003 *Chem. Mater.* **15** 4082
[37] Kang B and Ceder G 2009 *Nature* **458** 190
[38] Delacourt C, Laffont L, Bouchet R, Wurm C, Leriche J B, Morcette M, Tarascon J M and Masquelier C 2005 *J. Electrochem. Soc.* **152** A913
[39] Yonemura M, Yamada A, Takei Y, Sonoyama N and Kanno R 2004 *J. Electrochem. Soc.* **151** A1352
[40] Prosini P P, Lisi M, Zane D and Pasquali M 2002 *Solid State Ion.* **148** 45
[41] Amin R, Balaya P and Maier J 2007 *Electrochem. Solid-State Lett.* **10** A13
[42] Amin R, Lin C T and Maier J 2008 *Phys. Chem. Chem. Phys.* **10** 3524
[43] Peng B, Cogswell D A and Bazant M Z 2011 *Nano Lett.* **11** 4890
[44] Andersson A S, Kalska B, Häggström L and Thomas J O 2000 *Solid State Ionics* **130** 41
[45] Badi A P, Wagemaker M, Ellis B L, Singh D P, Borghols W J H, Kan W H, Ryan D H, Mulder F M and Nazar L F 2011 *J. Mater. Chem.* **21** 10085
[46] Andersson A S and Thomas J O 2001 *J. Power Sources* **498** 97
[47] Srinivasan V and Newman J 2004 *J. Electrochem. Soc.* **151** A1517
[48] Delmas C, Maccario M, Croguennec L, Cras F L and Weill F 2008 *Nat. Mater.* **7** 665
[49] Love C T, Korovina A, Patridge C J, Swider-Lyons K E, Twigg M E and Ramaker D E 2013 *J. Electrochem. Soc.* **160** A3153
[50] Delacourt C, Poizot P, Tarascon J M and Masquelier C 2005 *Nat. Mater.* **4** 254
[51] Dodd J L, Yazami R and Fultz B 2006 *Electrochem. Solid-State Lett.* **9** A151
[52] Van der Ven A, Garikipati K, Kim S and Wagemaker M 2009 *J. Electrochem. Soc.* **156** A949
[53] Chen G Y, Song X Y and Richardson T J 2006 *Electrochem. Solid-State Lett.* **9** A295
[54] Gu L, Zhu C B, Li H, Yu Y, Li C L, Tsukimoto S, Maier J and Ikuhara Y C 2011 *J. Am. Chem. Soc.* **133** 4661
[55] Orikasa Y, Maeda T, Koyama Y, Murayama H, Fukuda K, Tanida H, Arai H, Matsubara E, Uchimoto Y and Ogumi Z 2013 *J. Am. Chem. Soc.* **135** 5497
[56] Orikasa Y, Maeda T, Koyama Y, Murayama H, Fukuda K, Tanida H, Arai H, Matsubara E, Uchimoto Y and Ogumi Z 2013 *Chem. Mater.* **25** 1032
[57] Van Der Ven A, Bhattacharya J and Belak A A 2011 *Acc. Chem. Res.* **46** 1216
[58] Van der Ven A and Wagemaker M 2009 *Elecrochem. Commun.* **11** 881
[59] Sun Y, Lu X, Xiao R J, Li H and Huang X J 2012 *Chem. Mater.* **24** 4693
[60] Yu X Q, Wang Q, Zhou Y N, Li H, Yang X Q, Nam K W, Ehrlich S N, Khalid S and Meng Y S 2012 *Chem. Commun.* **48** 11537
[61] Weichert K, Sigle W, Aken P A V, Jamnik J, Zhu C B, Amin R, Acarturk T, Starke U and Maier J 2012 *J. Am. Chem. Soc.* **134** 2988
[62] Vandermarel C, Vinke G J B and Vanderlugt W 1985 *Solid State Commun.* **54** 917
[63] Sharma R A and Seefurth R N 1976 *J. Electrochem. Soc.* **123** C239
[64] Seefurth R N and Sharma R A 1977 *J. Electrochem. Soc.* **124** C136
[65] Seefurth R N and Sharma R A 1980 *J. Electrochem. Soc.* **127** 1101
[66] Wen C J and Huggins R A 1981 *J. Solid State Chem.* **37** 271

[67] Li H, Huang X J, Chen L Q, Zhou G, Zhang Z, Yu D, Mo Y J and Pei N 2000 *Solid State Ionics* **135** 181
[68] Limthongkul P, Jang Y I, Dudney N J and Chiang Y M 2003 *Acta Materialia.* **51** 1103
[69] Obrovacz M N and Christensen L 2004 *Electrochem. Solid-State Lett.* **7** A93
[70] Hatchard T D and Dahn J R 2004 *J. Electrochem. Soc.* **151** A838
[71] Key B, Bhattacharyya R, Morcrette M, Seznec V, Tarascon J M and Grey C P 2009 *J. Am. Chem. Soc.* **131** 9239
[72] Key B, Morcrette M, Tarascon J M and Grey C P 2011 *J. Am. Chem. Soc.* **133** 503
[73] Park C M, Kim J H, Kim H and Sohn H J 2010 *Chem. Soc. Rev.* **39** 3115
[74] Dimov N, Kugino S and Yoshio M 2003 *Electrochim. Acta* **48** 157
[75] Havenbergh K V, Turner S, Driesen K, Bridel J S and Tendeloo G V 2015 *Energy Technol.* **3** 699
[76] Wang C M, Li X, Wang Z, Xu W, Liu J, Gao F, Kovarik Li, Zhang J G, Howe J, Burton D J, Liu Z, Xiao X, Thevuthasan S and Baer D R 2012 *Nano Lett.* **12** 1624
[77] Li H, Zhu G Y, Huang X J and Chen L Q 2000 *J. Mater. Chem.* **10** 693
[78] Li H, Shi L, Lu W, Huang X and Chen L 2001 *J. Electrochem. Soc.* **148** A915